

Phase conjugation in the ocean: Experimental demonstration of an acoustic time-reversal mirror^{a)}

W. A. Kuperman, William S. Hodgkiss, and Hee Chun Song

*Marine Physical Laboratory, Scripps Institution of Oceanography, University of California, San Diego,
La Jolla, California 92093-0701*

T. Akal and C. Ferla

SACLANT Undersea Research Centre, La Spezia, Italy

Darrell R. Jackson

Applied Physics Laboratory, University of Washington, Seattle, Washington 98105

(Received 4 March 1997; accepted for publication 7 August 1997)

An experiment conducted in the Mediterranean Sea in April 1996 demonstrated that a time-reversal mirror (or phase conjugate array) can be implemented to spatially and temporally refocus an incident acoustic field back to its origin. The experiment utilized a vertical source–receiver array (SRA) spanning 77 m of a 125-m water column with 20 sources and receivers and a single source/receiver transponder (SRT) colocated in range with another vertical receive array (VRA) of 46 elements spanning 90 m of a 145-m water column located 6.3 km from the SRA. Phase conjugation was implemented by transmitting a 50-ms pulse from the SRT to the SRA, digitizing the received signal and retransmitting the time reversed signals from all the sources of the SRA. The retransmitted signal then was received at the VRA. An assortment of runs was made to examine the structure of the focal point region and the temporal stability of the process. The phase conjugation process was extremely robust and stable, and the experimental results were consistent with theory.

© 1998 Acoustical Society of America. [S0001-4966(97)00212-9]

PACS numbers: 43.10.Ln, 43.30.Vh, 43.30.Bp, 43.30.Hw, 43.30.Re [DLB]

INTRODUCTION

Phase conjugation is a process that has been first demonstrated in nonlinear optics¹ and more recently in ultrasonic laboratory acoustic experiments.^{2,3} Aspects of phase conjugation as applied to underwater acoustics also have been explored recently.^{4–7} The Fourier conjugate of phase conjugation is time reversal; implementation of such a process over a finite spatial aperture results in a “time-reversal mirror.”^{2,3,8} In this paper we describe an ocean acoustics experiment in which a time-reversal mirror was demonstrated.

In nonlinear optics, phase conjugation is realized using high intensity radiation propagating in a nonlinear medium. Essentially, the incident radiation imparts its own time dependence on the dielectric properties of the medium. The incident radiation is then scattered from this time-varying dielectric medium. The resulting scattered field is a time reversed replica of this incident field propagating in the opposite direction of the incident field. For example, the scattered field that results from an outgoing spherical wave is a spherical wave converging to the original source point; when it passes through the origin it has the time reversed signature of the signal which was transmitted from that point at the originating time. Clearly, this phenomenon can be thought of as a self-adaptive process, i.e., the process constructs a wavefront of the exact required curvature. (An alternative would be to use a concave spherical mirror with the precise radius of

curvature of the incident wavefront.) There is an assortment of nonlinear optical processes which can result in phase conjugation.¹ In acoustics, however, we need not use the propagation medium nonlinearities to produce a phase conjugate field.

Because the frequencies of interest in acoustics are orders of magnitude lower than in optics, phase conjugation can be accomplished using signal processing. As in the optical case, phase conjugation takes advantage of reciprocity which is a property of wave propagation in a static medium and is a consequence of the invariance of the linear lossless wave equation to time reversal. In the frequency domain, time reversal corresponds to conjugation invariance of the Helmholtz equation. The property of reciprocity allows one to retransmit a time reversed version of a multipath dispersed probe pulse back to its origin, arriving there time reversed, with the multipath structure having been undone.^{8,9} This process is equivalent to using the ocean as a matched filter since the probe pulse arrival has embedded in it the transfer function of the medium. This process can be extended further by receiving and retransmitting the probe signal with a source–receiver array. Depending on the spatial extent of the array, the above process results in some degree of spatial focusing of the signal at the origin of the probe signal.

A time-reversal mirror (TRM) can therefore be realized with a source–receiver array. The incident signal is received, time reversed, and transmitted from sources contiguous with the receiving hydrophones. The time reversal can be accomplished in a straightforward way, for example, by using the rewind output of an analog tape recorder or by a simple

^{a)}“Selected research articles” are ones chosen occasionally by the Editor-in-Chief that are judged (a) to have a subject of wide acoustical interest, and (b) to be written for understanding by broad acoustical readership.

program that reverses a digitized segment of a received signal.

An acoustic TRM has already been demonstrated in an ultrasonic laboratory using an array of source/receiver transducers (SRA).³ The array length was 10 cm and a single 4-MHz source was placed at a transverse distance of 5 cm together with another receive array. The single source transmitted a probe pulse which was received at the SRA; the received pulse was time reversed and retransmitted from the SRA and subsequently received at an array (with the same orientation as the SRA) near the single source. The results showed a 15-dB peak at the location of the source relative to sidelobes away from the probe source location. Note that this focal point was at a range one-half the size of the aperture.

Phase conjugation (PC) or the implementation of a TRM in the ocean is relevant to recent trends in acoustic signal processing which have emphasized utilizing knowledge of the environment, e.g., matched field processing (MFP).¹⁰ However, MFP requires accurate knowledge of the environment throughout the propagation path, which of course is difficult or impossible to obtain. Phase conjugation is an environmentally self-adaptive process which may therefore have significant applications to localization and communications in complicated ocean environments. Although the “effective” ocean environment must remain static over the turn around time of the PC process, ocean variability on time-scales shorter than the turn around time might be compensated for with feedback algorithms. However, an understanding of relevant ocean time scales *vis a vis* the stability of the PC process will be required.

In this paper we describe an April 1996 experiment in which an acoustic TRM was demonstrated in the ocean. In this initial experiment, a focal range of about 100 times the SRA aperture was accomplished easily with a 445-Hz probe source, a water depth of the order of 100 m, and a focal range of about 6.3 km. Large focal distances are obtainable in the ocean because in a waveguide geometry, a SRA has images which increase its effective aperture. Hence, there is an advantage to having a waveguide geometry over a free-field environment as was used first in the ultrasonic laboratory experiment. Measurements in this first low-frequency ocean experiment also suggest a temporal stability of the PC process which is longer than what was expected intuitively. Some quantitative results on this stability are presented.

In the next section we review the relevant theoretical issues including some simulation results leaving the details to an Appendix and appropriate references. Section II describes the experiment in which the TRM was demonstrated and Sec. III presents the results.

I. BACKGROUND THEORY AND SIMULATION FOR THE TRM EXPERIMENT

The theory of phase conjugation *vis a vis* ocean acoustics already has been presented.⁴⁻⁷ Here we briefly review salient issues using the basic geometry of the TRM experiment (shown schematically in Fig. 2). More detail on theory is given in Appendix A and some additional details concerning experimental equipment are given in Appendix B.

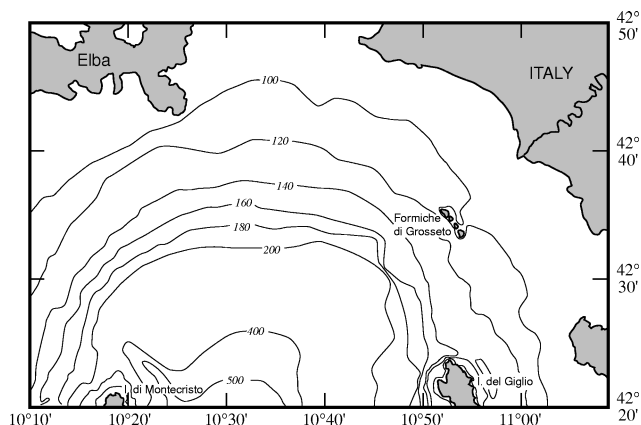


FIG. 1. Location of phase conjugation experiment. A source/receiver array (SRA) was deployed in 125-m-deep water and cabled approximately 1 km back to a small island, Formica Grande, the northernmost island of Formiche di Grosseto (42° 34.6' N, 10° 52.9' E). A rf telemetered vertical receive array (VRA) was deployed in 145-m-deep water approximately 6.3 km west of Formica.

A. Experimental geometry

The TRM experiment was performed off the west coast of Italy in April 1996 as indicated in Fig. 1. Figure 2 is a schematic of the experiment and indicates the types of environmental measurements that were made. The TRM was implemented by a 77-m source-receiver array (SRA) in 125-m-deep water which was hardwired to the Isola di Formica di Grosseto. The SRA consisted of 20 hydrophones with 20 contiguously located slotted cylinder sources with a nominal resonance frequency of 445 Hz. The sources were operated at a mean nominal 165-dB source level. The received signals were digitized, time reversed, and after being converted back to analog form, retransmitted. A probe source (PS) of the same type used in the SRA was deployed from the NATO research vessel ALLIANCE. The probe source together with a hydrophone was also used in parts of the experiment as a transponder. The ALLIANCE also deployed a vertical 46 element receive array (VRA) spanning 90 m located 6.3 km from the SRA which radio telemetered all individual element data back to the ALLIANCE. Ideally, the PS should be in the vertical SRA-VRA plane to correspond perfectly to the simulations in the following section; for practical reasons the PS was placed a few tenths of a km out of this plane. This did not introduce a significant error because the bathymetry

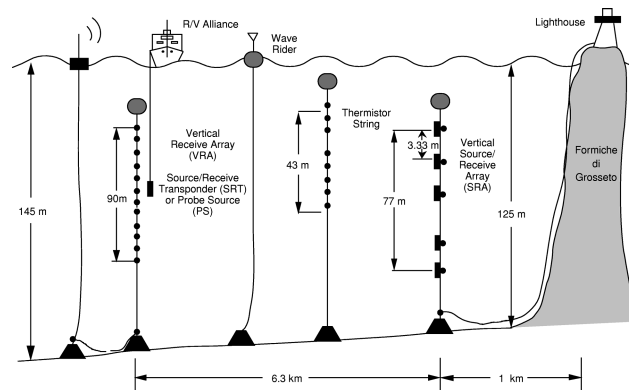


FIG. 2. Experimental setup of the phase conjugation experiment.

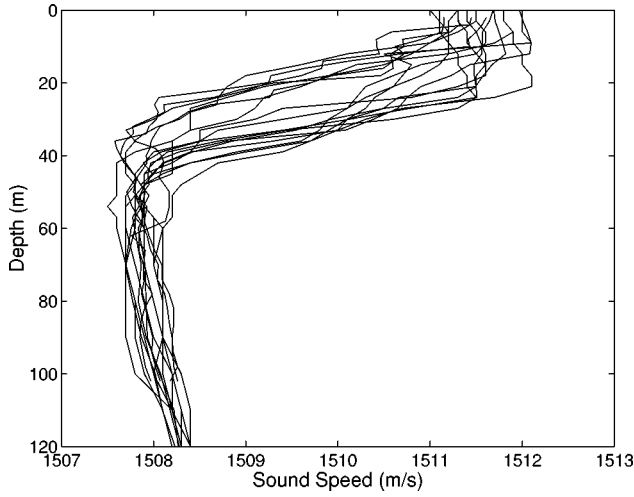


FIG. 3. Collection of sound-speed profiles from CTDs taken during the experiment.

was flat in the vicinity of the VRA. Figure 3 is a collection of the sound speed profiles (SSP's) obtained from the conductivity–temperature–depth probe (CTD) as an indication of the variability over the duration of the experiment. The bottom sound-speed structure as determined from earlier experiments¹¹ is shown in Fig. 4(a). More details on the instrumentation and processing are given in Appendix B.

B. Overview of theory

For simplicity in this subsection, we analytically summarize the basics of phase conjugation in a range-independent waveguide. The simulations and comparisons with experimental data presented later on in the paper will include range-dependent modeling. The source, PS, is located a horizontal distance R from the source/receive phase conjugate array, SRA.

1. Harmonic excitation

The acoustic field, $G_\omega(R; z_j, z_{ps})$, at the j th receiver element of the SRA from the point source PS in Fig. 2 is determined from the Helmholtz equation¹² [assuming a harmonic time dependence of $\exp(-i\omega t)$]

$$\begin{aligned} \nabla^2 G_\omega(\mathbf{r}; z, z_{ps}) + k^2(z) G_\omega(\mathbf{r}; z, z_{ps}) \\ = -\delta(\mathbf{r} - \mathbf{r}_{ps}) \delta(z - z_{ps}), \quad k^2(z) = \frac{\omega^2}{c^2(z)}, \end{aligned} \quad (1)$$

where z is taken positive downward and $\mathbf{r} = (x, y)$. Letting r be the horizontal distance from the probe source, Eq. (1) has the far field, azimuthally symmetric normal mode solution for pressure given by

$$\begin{aligned} G_\omega(r; z, z_{ps}) = \frac{i}{\rho(z_{ps})(8\pi r)^{1/2}} \exp(-i\pi/4) \\ \times \sum_n \frac{u_n(z_{ps})u_n(z)}{k_n^{1/2}} \exp(ik_n r), \end{aligned} \quad (2)$$

where u_n, k_n are the normal mode eigenfunctions and modal wave numbers obtained by solving the following eigenvalue problem with well-known boundary conditions:¹²

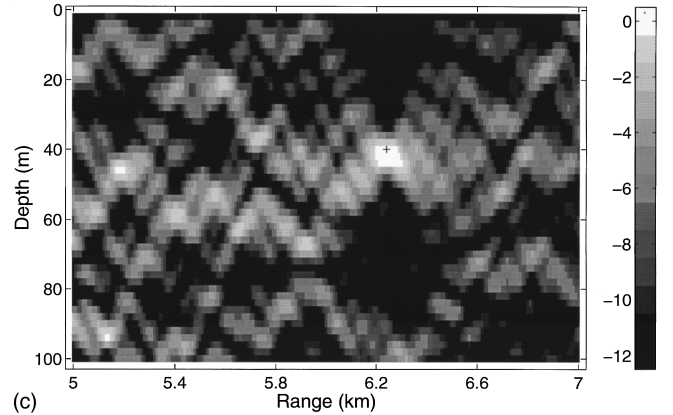
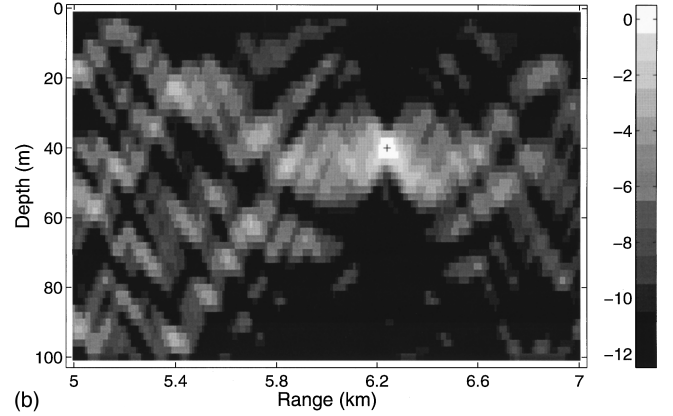
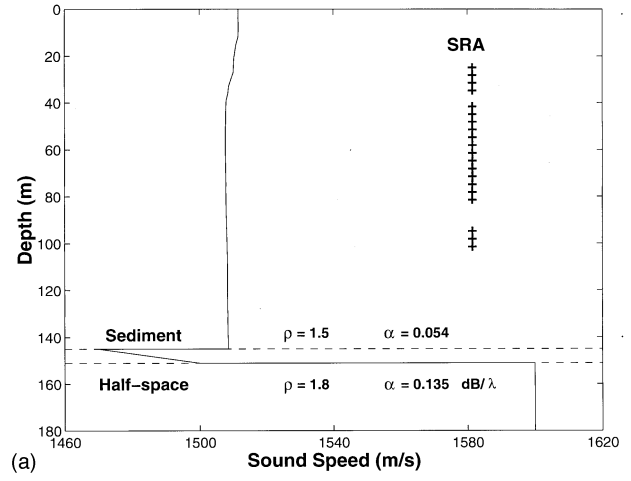


FIG. 4. Single frequency simulation of phase conjugation for the geometry of Fig. 2 for a probe source located at a depth of 40 m and a range of 6.3 km. (a) Sound-speed profile. The density, ρ and attenuation, α (in dB/wavelength) of the bottom two layers are also given. (b) Simulation for a 20-element SRA. Note the sharp focus in depth. (c) Simulation for only the bottom 10 elements of the SRA.

$$\frac{d^2 u_n}{dz^2} + [k^2(z) - k_n^2] u_n(z) = 0. \quad (3)$$

The mode functions form a complete set (for simplicity we omit discussion of the continuous spectrum though a good approximation is to use a set of discrete mode functions obtained from a waveguide extended in depth and terminated by a pressure release or rigid boundary)

$$\sum_{\text{all modes}} \frac{u_n(z)u_n(z_s)}{\rho(z_s)} = \delta(z - z_s), \quad (4)$$

and satisfy the orthonormality condition

$$\int_0^\infty \frac{u_m(z)u_n(z)}{\rho(z)} dz = \delta_{nm}, \quad (5)$$

where δ_{nm} is the Kronecker delta symbol.

The received field at the source/receiver array (SRA) at range R from PS with source/receive elements at depths z_j , is $G_\omega(R; z_j, z_{ps})$. The phase conjugation process consists of exciting the SRA sources by the complex conjugate of the received field, $G_\omega^*(R; z_j)$. The resulting acoustic field transmitted from the J sources satisfies the wave equation,

$$\nabla^2 P_{pc}(r, z) + k^2(z)P_{pc}(r, z) = \sum_{j=1}^J \delta(z - z_j)G_\omega^*(R; z_j, z_{ps}), \quad (6)$$

where the range r is with respect to the SRA. Using Green's function theory, the solution of Eq. (6) is the volume integral of the product of the Green's function as specified by Eq. (1) and the source term of Eq. (6). For a vertical line of discrete sources, the integral reduces to a sum over the source positions,

$$P_{pc}(r, z; \omega) = \sum_{j=1}^J G_\omega(r; z, z_j)G_\omega^*(R; z_j, z_{ps}), \quad (7)$$

where R is the horizontal distance of the SRA from PS and r is the horizontal distance from the SRA to a field point.

Note that the magnitude squared of the right-hand side (rhs) of Eq. (7) is the ambiguity function of the Bartlett matched-field processor¹⁰ (with an appropriate normalization factor) where the data are given by $G_\omega(R; z_j, z_{ps})$ and the replica field by $G_\omega(r; z, z_j)$. In effect, the process of phase conjugation is an implementation of matched-field processing where the ocean itself is used to construct the replica field. Or, alternatively, matched-field processing simulates the experimental implementation of phase conjugation in which a source/receive array is used. To demonstrate that $P_{pc}(r, z)$ focuses at the position of the probe source, (R, z_{ps}) , we simply substitute Eq. (2) into Eq. (7) which specifies that we sum over all modes and array sources

$$P_{pc}(r, z; \omega) \approx \sum_m \sum_n \sum_j \frac{u_m(z)u_m(z_j)u_n(z_j)u_n(z_{ps})}{\rho(z_j)\rho(z_{ps})\sqrt{k_m k_n} r R} \times \exp i(k_m r - k_n R). \quad (8)$$

For an array which substantially spans the water column and adequately samples most of the modes, we may approximate the sum of sources as an integral and invoke orthonormality as specified by Eq. (5). Then the sum over j selects out modes $m = n$ and Eq. (8) becomes

$$P_{pc}(r, z; \omega) \approx \sum_m \frac{u_m(z)u_m(z_{ps})}{\rho(z_{ps})k_m \sqrt{rR}} \exp i k_m (r - R). \quad (9)$$

The individual terms change sign rapidly with mode number. However, for the field at PS, $r = R$, the closure relation of Eq. (4) can be applied approximately (we assume that the

k_n 's are nearly constant over the interval of the contributing modes) with the result that $P_{pc}(r, z) \approx \delta(z - z_{ps})$. Figure 4 is a simulation of the phase conjugation process using Eq. (7) for a probe source at 40-m depth and at a range of 6.3 km from a 20 element SRA as specified in Fig. 2 verifying the above discussion. Range-dependent bathymetry was used as the input to an adiabatic mode model¹³ for the specific sound-speed profile taken from the ensemble of profiles in Fig. 3 and a bottom sound-speed structure shown in Fig. 4(a) which includes a low speed layer as has been ascertained experimentally.¹¹ Notice that the focusing in the vertical is indicative of the closure property of the modes. As a matter of fact, for an SRA with substantially fewer elements, we see that the focusing still is relatively good. For example, Fig. 4(c) also shows a result for the bottom 10 elements of the SRA which are below the thermocline.

2. Pulse excitation

In this experiment a 50-ms pure-tone pulse with center frequency 445 Hz was used for the probe transmission. We can Fourier synthesize the above results to examine phase conjugation for pulse excitation. Here, in the context of this experiment, we remind the reader that phase conjugation in the frequency domain is equivalent to time reversal in the time domain. The j th element of the SRA receives the following time-domain signal, given by Fourier synthesis of the solution of Eq. (1):

$$P(R, z_j; t) = \int G_\omega(R; z_j, z_{ps})S(\omega)e^{-i\omega t} d\omega, \quad (10)$$

where $S(\omega)$ is the Fourier transform of the probe source pulse. This expression incorporates all waveguide effects, including time elongation due to multipath propagation. For convenience, take the time origin such that $P(R, z_j; t) = 0$ outside the time interval $(0, \tau)$. Then the time reversed signal that will be used to excite the j th transmitting element of the SRA is $P(R, z_j; T - t)$ such that $T > 2\tau$. This condition is imposed by causality; the signal has to be completely received before it can be time reversed. Then

$$\begin{aligned} P(R, z_j; T - t) &= \int G_\omega(R; z_j, z_{ps})S(\omega)e^{-i\omega(T-t)} d\omega \\ &= \int [G_\omega^*(R; z_j, z_{ps})e^{i\omega T}S^*(\omega)]e^{-i\omega t} d\omega, \end{aligned} \quad (11)$$

where the sign of the integration variable, ω , has been reversed and the conjugate symmetry of the frequency-domain Green's function and probe pulse has been used. The quantity in brackets in Eq. (11) is the Fourier transform of the signal received by the j th SRA receiver element after time reversal and time delay. Hence there is an equivalence of time reversal and phase conjugation in their respective time and frequency domains.

Noting that the bracketed quantity in Eq. (11) is the frequency-domain representation of the signal retransmitted by the j th element of the SRA, Fourier synthesis can be used to obtain the time-domain representation of the field produced by the TRM. Using Eq. (7),

$$P_{pc}(r, z; t) = \sum_{j=1}^J \int G_{\omega}(r, z, z_j) G_{\omega}^*(R, z_j; z_{ps}) e^{i\omega T} \times S^*(\omega) e^{-i\omega t} d\omega. \quad (12)$$

This expression can be used to show that the TRM produces focusing in time as well as in space. Focusing in time occurs because a form of matched filtering occurs. To understand this, examine the TRM field at the focus point [that is, take $r=R$, $z=z_{ps}$ in Eq. (12)]. Neglecting density gradients, reciprocity allows the interchange $G_{\omega}(R, z_{ps}, z_j) = G_{\omega}(R, z_j, z_{ps})$. Then the time-domain equivalent of Eq. (12) is

$$P_{pc}(r, z; t) = \frac{1}{(2\pi)^2} \int \sum_{j=1}^J \left[\int G_{t'+t''}(R, z_j, z_{ps}) \times G_{t'}(R, z_j, z_{ps}) dt' \right] S(t''-t+T) dt'', \quad (13)$$

where the time-domain representations of the Green's function and probe pulse are used. Note that the Green's function is correlated with itself. This operation is matched filtering, with the filter matched to the impulse response for propagation from the probe source to the j th SRA element. This operation gives focusing in the time domain, that is, it reduces the time elongation due to multipath propagation.⁸ The sum over array elements is a form of spatial matched filtering, analogous to that employed in the Bartlett matched-field processor.¹⁰ In addition, this sum further improves temporal focusing as the temporal sidelobes of the matched filters for each channel tend to average to zero which also is analogous to broadband matched-field processing results.¹⁴ Finally, note that the integral over t'' in Eq. (13) is a convolution of each matched-filtered channel impulse response with the time-reversed and delayed probe pulse. As a consequence, this pulse is *not* matched filtered, for example, a linear FM up-sweep will appear as a down-sweep at the focus and will not be compressed.

Figure 5(a) shows a simulation for a 50-ms rectangular pulse with center frequency 445 Hz for the same geometry used in Fig. 4(a) as received at the SRA and Fig. 5(b) shows the pulse as transmitted to a plane at a range of 6.3 km, the range of PS. Four sources were excluded from the simulation because these phones were not used in the experiment. Note the temporal focusing; that is, the 50-ms pulse disperses to about 75 ms at the SRA but the time reversed pulse received at the VRA is compressed (focused) to 50 ms as opposed to exhibiting even further time dispersion. On the other hand, Fig. 5(c) shows a pulse 500 m outbound of PS (i.e., the VRA is at the same location but PS is 500 m closer to the SRA). The pulse is not spatially focused and it is temporally more diffuse than the result for the focal spot.

3. Properties of the focal region

A detailed discussion of the spatial and temporal factors affecting the focus is given in Appendix A. The primary result is that the TRM focus is robust, provided the SRA adequately samples the field in the water column. First, the focus tends to depend primarily on the properties of the

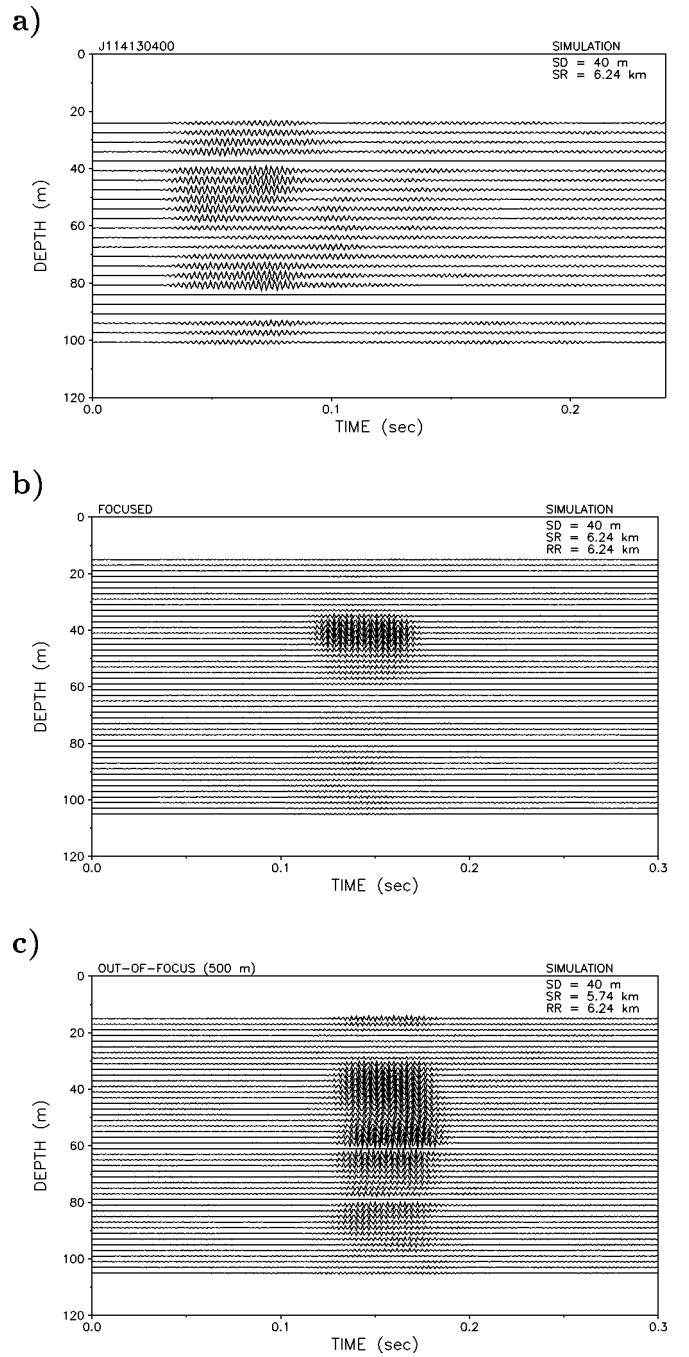


FIG. 5. Simulation of a 445-Hz, 50-ms transmitted pulse for the geometry in Fig. 2 for a probe source located at a depth of 40 m. (a) Pulse received on the SRA at range of 6.3 km from PS. There is a temporal dispersion of about 75 ms and significant energy throughout the water column. (b) The focus of the time reversed pulse at the VRA. There is pulse compression back to the original transmitted 50-ms duration as well as spatial focusing in depth. (c) Vertical and temporal distribution for a pulse 500 m outbound of PS (the VRA is at the same location but PS is 500 m closer to the SRA).

ocean near the focus and tends to be independent of (the possibly range-dependent) properties of the medium between the SRA and the focus. Temporal changes in the medium due to, for example, surface waves and internal waves degrade the focus, but this degradation will be tolerable if the average (or coherent) Green's function is not severely reduced by these time variations. Generally, the shape of the focus is approximated by the field that a point source placed at the

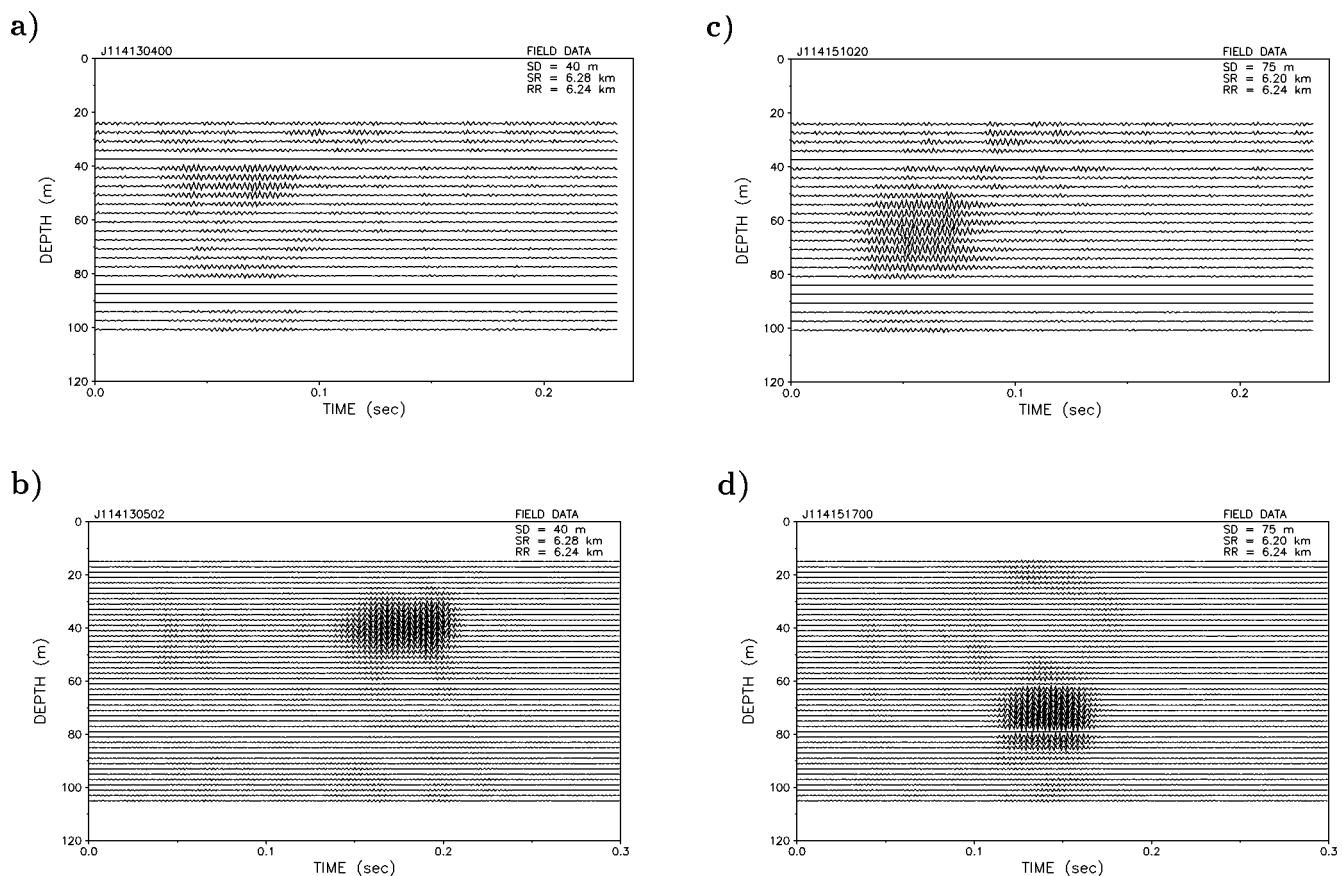


FIG. 6. Experimental results for probe source PS and VRA at same range. (a) The pulse data received on the SRA for PS at depth of 40 m. (b) The data received on the VRA from the time reversed transmission of pulses shown in (a). The VRA is 40 m inbound from the focus as determined by DGPS. (c) The pulse data received on the SRA for PS at depth of 75 m. (d) The data received on the VRA from the time-reversed transmission of pulse shown in (c). The VRA is 40 m outbound from the focus as determined by DGPS.

focus generates after nonpropagating modes are subtracted. Thus if absorption or scattering tends to eliminate high-order modes, the focus will be comprised of the remaining lower order modes and will be relatively broader. Very roughly, the vertical width of the focus will be equal to the water depth (or depth of the duct) divided by the number of contributing modes if the sound speed (in the duct) is not strongly dependent on depth.

The TRM focus is also robust with respect to array shape⁴ provided the shape does not change between the probe reception and time reversed transmission. This property makes it unnecessary to know the exact shape of the TRM array and offers a considerable advantage over conventional beamforming.

II. EXPERIMENTAL DEMONSTRATION OF A TRM IN THE OCEAN

An assortment of runs was made to examine the structure of the focal point region and the temporal stability of the process. Here we will be reporting on three types of experiments (note that range refers to the distance from the SRA):

(1) Demonstration of the time-reversal mirror (TRM) in the ocean. The probe source (PS) is moved from shorter range to a longer range past the VRA. At each PS range, it sends out a 445-Hz, 50-ms pulse on the even minute. The pulse is received at the SRA, time reversed and retransmitted

five times (once every 10 s) starting at the odd minute. This signal is received at the VRA and data from all channels are recorded. Note that when PS is at the same range of the VRA, the data recorded at the VRA are a vertical slice of the focal range as indicated in the simulation for a harmonic source in Fig. 4. Figure 5(b) is a simulation of the expected results at that range. When PS is closer than the VRA, the VRA data correspond to a measurement beyond the focal range and vice versa when PS is beyond the VRA.

(2) Stability of TRM. PS is at the VRA range which means that we are measuring the vertical profile of the focal region. A 50-ms, 445-Hz pulse is sent out once and the SRA retransmits the same time reversed signal every 10 s for an extended period. Here the goal is to determine how long a single probe signal remains a valid phase conjugate probe for the specific ocean environment and source location. These results are constrained by the limitations of the actual experiment.

(3) Acoustic ping pong. The probe source with collocated receiver now acts as a transponder. The SRA transmits a 50-ms water column filling signal to the transponder which is at a depth of 75 m. The transponder retransmits the received signal (no time reversal) to the SRA which then transmits the time-reversed signals from the full array. This commences an acoustic ping pong iteration between SRA and PS with PS acting as a transponder (SRT).

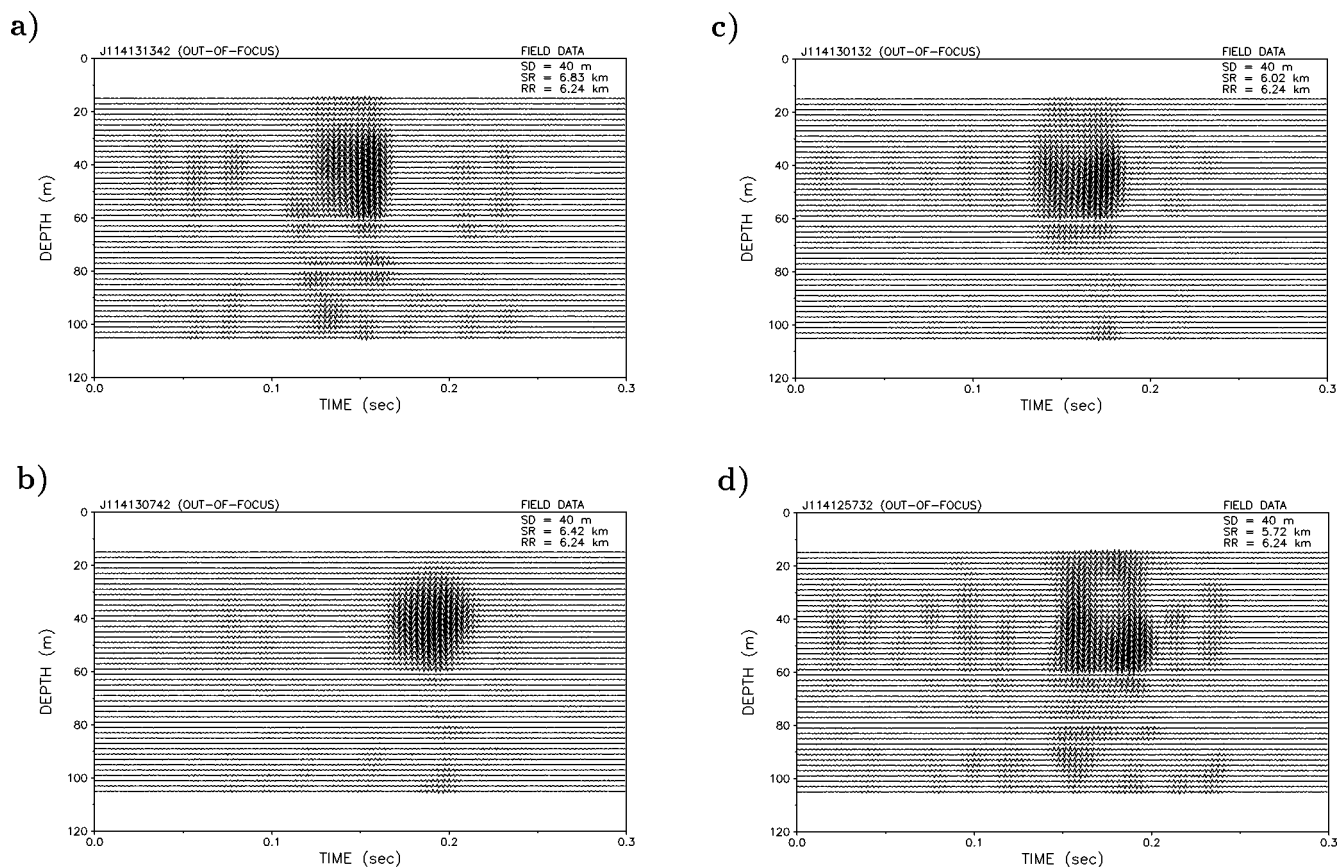


FIG. 7. Out of focus data received on the VRA from the time-reversed transmission of pulses with PS at a depth of 40 m. (a) PS is outbound 600 m. (b) PS is outbound 200 m. (c) PS is inbound 200 m. (d) PS is inbound 500 m.

A. Demonstration of TRM in the ocean

The vertical receive array VRA was deployed at a range, determined by DGPS, of 6.24 km from the SRA and the probe source PS was deployed at two different depths, 40 m and 75 m. Figure 6 shows the pulse as received on the SRA and VRA for both source depths. The data at the SRA are a combination of signal and noise. A 233-ms window was digitized and time reversed for transmission to the VRA. When the VRA and PS have the same range (experimentally within 40 m by a DGPS measurement) to the SRA, we see the focusing as predicted in Sec. I for a probe source at 40 m depth and similar results for a probe source at 75-m depth. Clearly, we have implemented a time-reversal mirror focusing at the range and depth of the probe source.

Figure 7 shows the result as we sweep through the focal point. Note that because of the way the experiment had to be performed, we are actually keeping the VRA fixed and changing the range of PS. An alternative way to present the focusing effect which displays the sidelobes off the main peak is shown in Fig. 8. The solid line with circles is the nearest to the focal region. Here we see the sidelobes in the vertical becoming large as we move away from the focal region.

B. Stability of TRM

The variability of the sound-speed structure in the water column is indicated in Fig. 3 which contains a collection of

sound speeds derived from CTD's at different positions and times throughout the experiment. A thermistor chain placed at the position indicated in Fig. 2 reveals the varying temperature structure as shown in Fig. 9. In addition, there is information concerning wave heights from the waverider shown in Fig. 2. The time series of the rms waveheight is

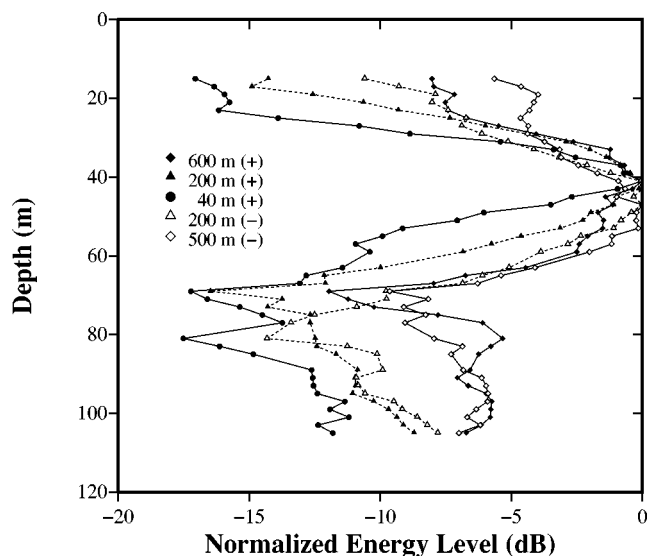


FIG. 8. The energy over a 0.3-s window as a function of depth for various ranges from the focal region. The depth of the probe source was 40 m. + means VRA is outbound from the focus (PS).

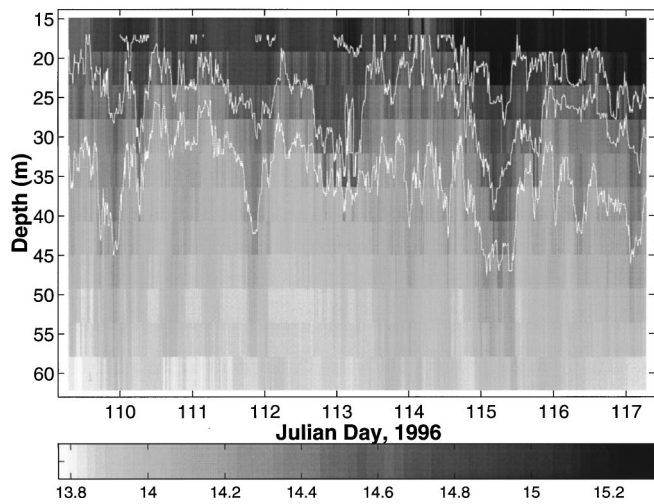


FIG. 9. Thermistor chain data. The contours from the top down are 15, 14.6, and 14.2 °C.

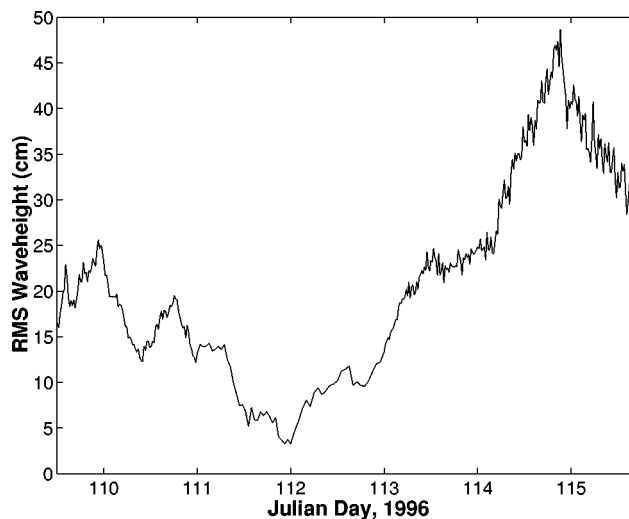
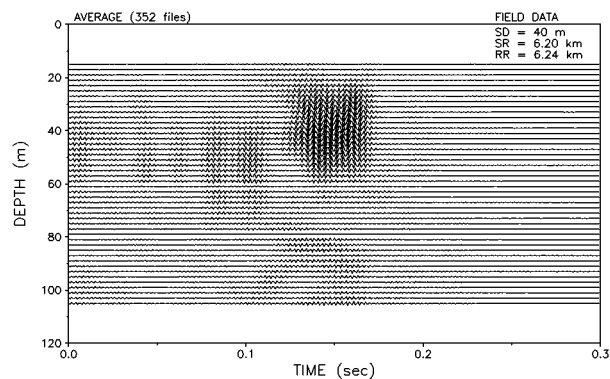
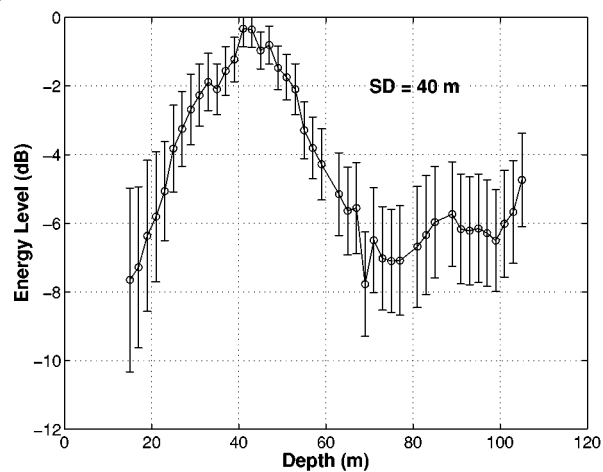


FIG. 10. Surface waveheight measurements from the waverider.

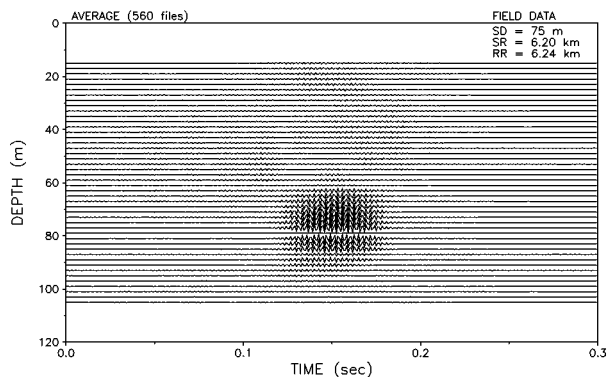
a)



c)



b)



d)

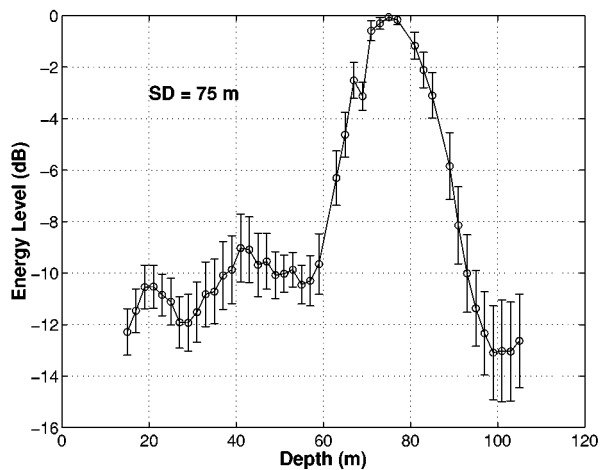


FIG. 11. Results on stability of the focal region. (a) Pulse arrival structure at VRA for probe source at 40 m depth averaged over 1 h. (b) Pulse arrival structure at VRA for probe source at 75 m depth averaged over 2 h. (c) Mean and standard deviation of energy in a 0.3-s window for 40-m probe source. (d) Mean and standard deviation of energy in a 0.3-s window for 75-m probe source.

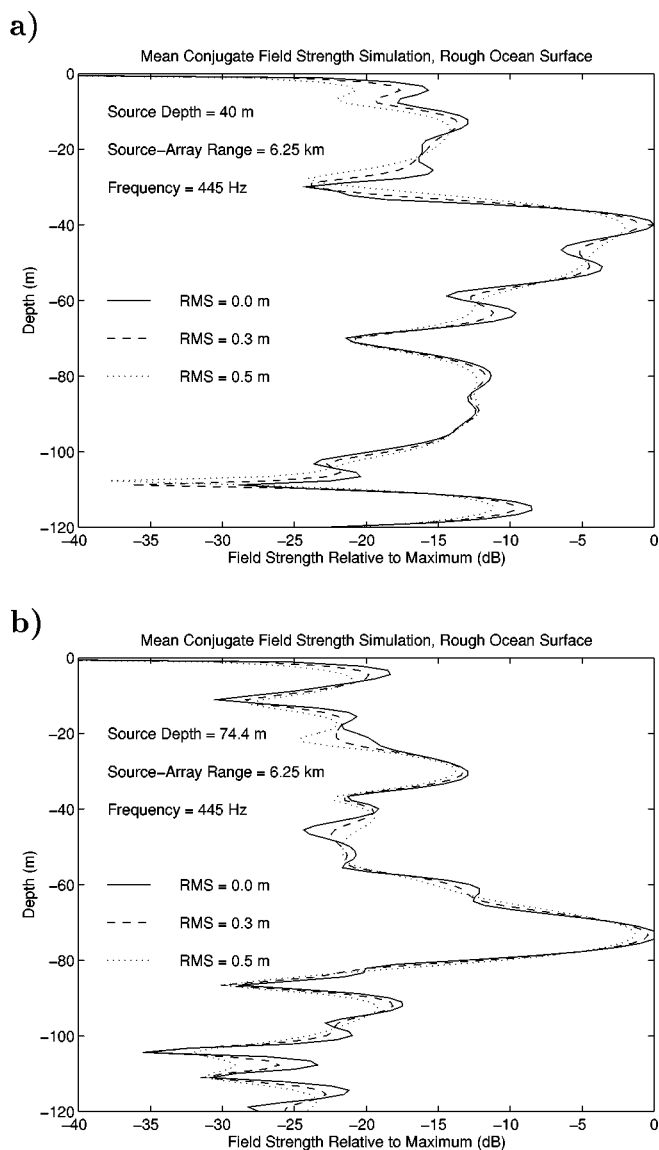


FIG. 12. Simulation of vertical profile of the mean field at the focal range for different values of surface roughness. (a) Probe source at 40 m. (b) Probe source at 75 m.

shown in Fig. 10. Although the time series of the environmental data does not have the temporal and spatial resolution for an exhaustive comparison of theory and data, the two stability data collection periods show qualitative agreement with a first order analysis of the nature of the fluctuations.

Basically, as shown in Appendix A, theory predicts that the mean field dominates the focal region with fluctuations, being a diffuse phenomenon, becoming more apparent away from the focus. That is, if one considers the total field to be composed of a mean field and a fluctuating field, it is the mean field which has the coherence properties which produce the focusing whereas the fluctuating field is a form of signal-generated noise.

Two stability data collection periods for the probe source depths of 40 m and 75 m were made for 1 h and 2 h, respectively (the lengths of the runs were dictated by experimental circumstance). The Julian day and times of the stability runs for SD=75 m and SD=40 m were J114 15:11–

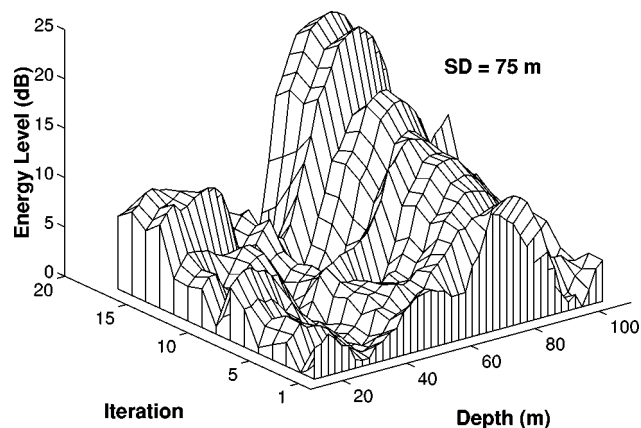


FIG. 13. Acoustic ping pong between a transponder at 75 m depth and a range of 6.24 km from the SRA. The waterfall plot shows the energy in a 0.3-s window at the VRA (which is at the same range as the transponder) as a function of depth for each of the 15 round trips. There were two minutes between each round trip.

17:07 and J114 18:47–19:47, respectively. Figure 11 shows the results of these runs. These plots indicate that the focus was considerably more stable for the deep probe source versus the shallower probe source and that the focus is broader for the shallower probe source.

Simulations using representative rms wave heights from Fig. 10 and the environment of the experiment with a normal mode rough surface mean field scattering theory¹⁵ are shown in Fig. 12. The results indicate that surface scattering does not have a significant impact on the focal region for this particular environment. On the other hand, examination of the environmental data indicates that the probe source at the shallower depth was at the bottom of the thermocline where the water column variability was the greatest. As derived in Appendix A, we expect the focusing phenomenon to be most sensitive to the environment at the endpoints of the experimental geometry. The tentative conclusion is that the fluctuations in this case were caused by sound-speed fluctuations in the water column, but more analysis and finer sampled volume data are required.

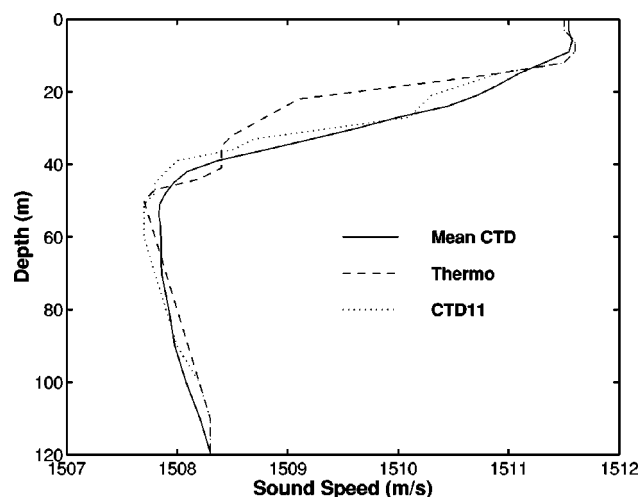


FIG. 14. Sound-speed profiles. The solid line was the optimum profile from the inversion process. The dashed line is thermistor chain derived sound-speed closest in time to the data shown in Fig. 6(a),(b).

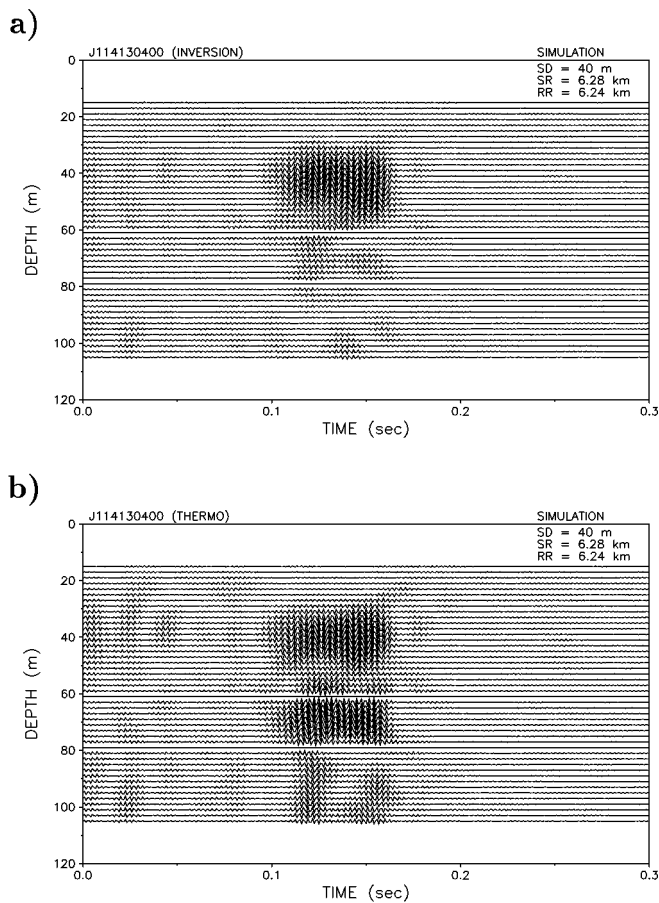


FIG. 15. Backpropagation using data from the SRA for the probe source at a depth of 40 m. (a) From the inversion process. (b) From the profile measured at the time of the experiment.

C. Acoustic ping pong: iterative focusing

The purpose of the acoustic ping pong experiment is to demonstrate that focusing can be iteratively improved. This has already been demonstrated and explained in earlier free-field multiscatterer, ultrasonic experiments.^{16–18} Basically, since a TRM returns signals to their origin in proportion to their original relative strengths, repeating the process a second time will reduce the level of the focused field for the weaker signals versus the stronger signals, and so on. The theoretical explanation is in terms of eigenvalues and eigenvectors of the time-reversal operator. Eventually, only the strongest signal (or that part of the field corresponding to the largest eigenvalue) is focused.

In this experiment, ping pong was initiated and kept going for 15 round trips. Figure 13 is a waterfall plot of the energy in a 0.3-s window of the pulses received on the VRA which was at the same range as the transponder. There are 2 min between each round trip.

These results show the increased focusing brought about by the iteration process. However, this single source result is not completely analogous to the free-space multiscatterer results in Refs. 16–18. Rather, it depends on the particular TRM array-data eigenvector structure in the specific waveguide environment. A paper with a detailed explanation of this process is in preparation.

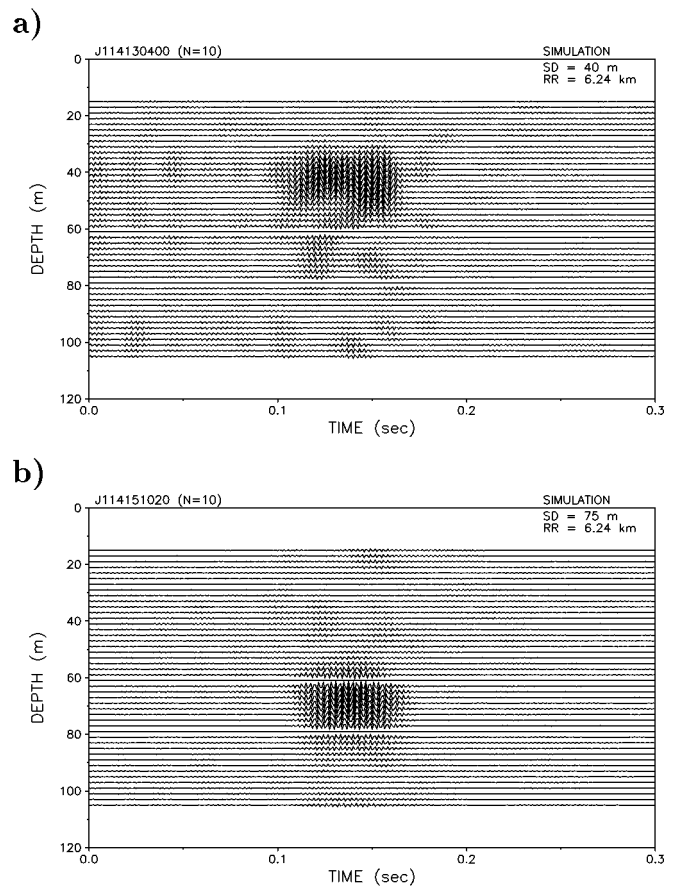


FIG. 16. Backpropagation using data from every other element of the SRA: 10-element TRM. (a) Probe source at a depth of 40 m. (b) Probe source at a depth of 75 m.

III. EXTRAPOLATING THE EXPERIMENTAL RESULTS

We have demonstrated that a time reversal mirror (TRM) can be implemented in the ocean and that its performance is consistent with theory. In this section we use a combination of data and theory to gain some additional insight into the potential usefulness of this process. In particular, we examine:

- (1) its potential as a tool for inversion;
- (2) whether a smaller aperture or few source/receiver elements would still be effective for producing a TRM.

Further, we use item 1 to help estimate the TRM performance of a smaller SRA.

A. TRM applied to sound speed inversion

Empirical orthogonal functions¹⁹ (EOFs) about the mean of the profiles shown in Fig. 3 were constructed. It was then found through trial and error that the mean profile was sufficient to provide the optimum focusing using simulated backpropagation from the SRA data. That is, the coefficient of the first term of an EOF expansion was negligible with respect to the expected accuracy of the sound-speed profiles. A plot of this result compared to “CTD 11” which was used in the simulations in Sec. I is shown in Fig. 14. This procedure is akin to matched field tomography^{10,20,21} except that more information is available because of the vertical array at the

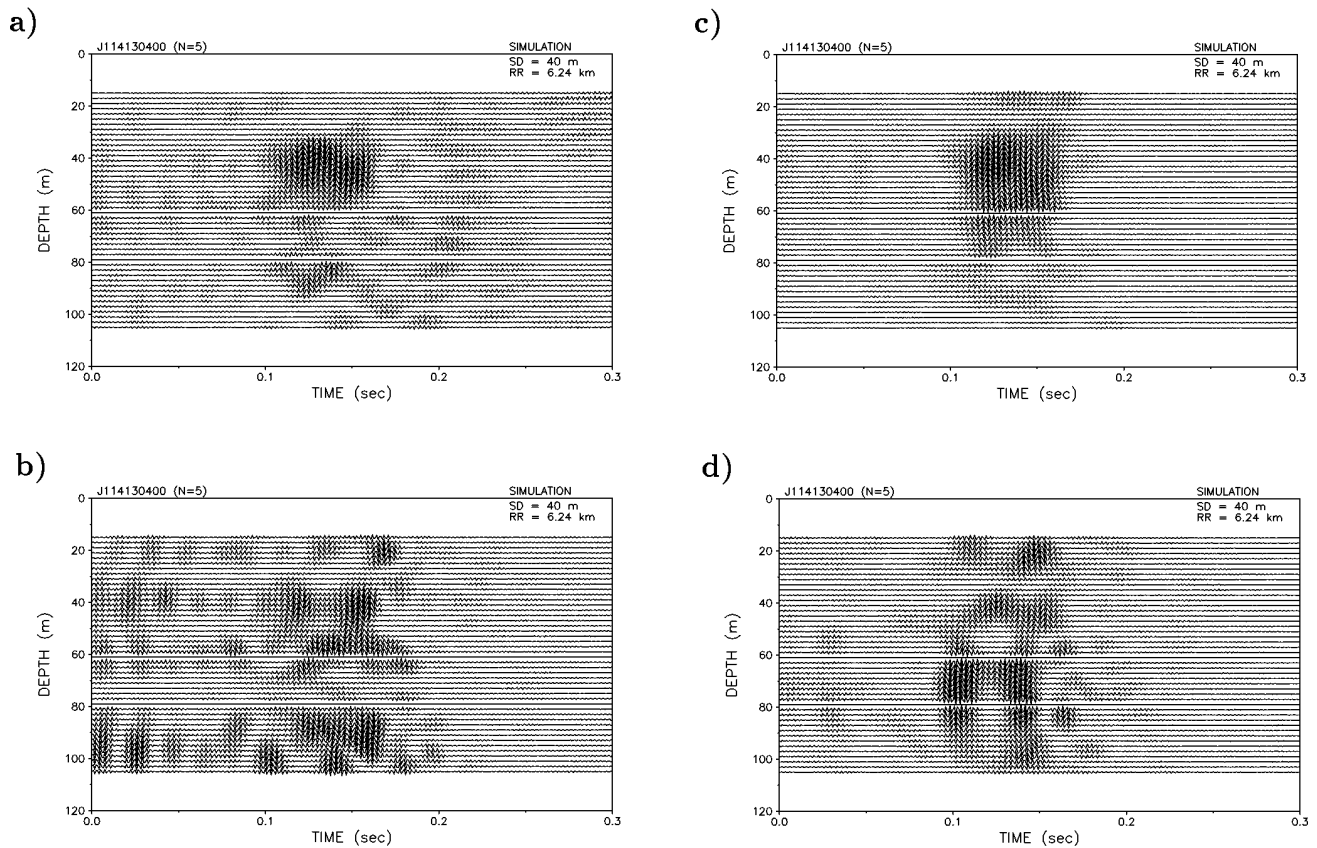


FIG. 17. Backpropagation produced TRM from a five-element SRA for the probe source at 40 m. (a) Elements 1, 5, 9, 13, 17 as numbered from the top. (b) First quarter of SRA. (c) Second quarter of SRA. (d) Third quarter of SRA.

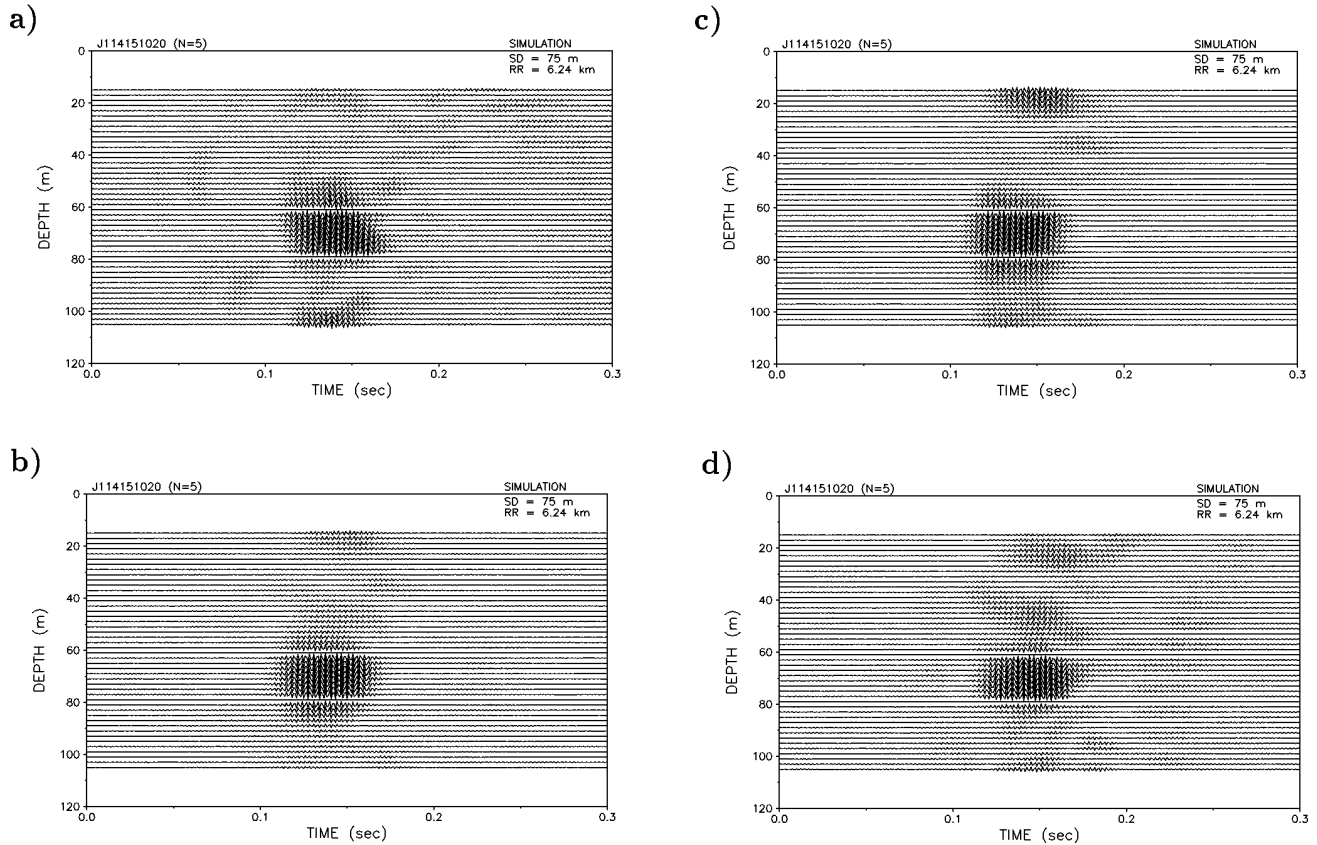


FIG. 18. Backpropagation produced TRM from a five-element SRA for the probe source at 75 m. (a) Elements 1, 5, 9, 13, 17 as numbered from the top. (b) Elements 12, 14, 16, 18, 20. (c) Third quarter of SRA. (d) Lowest quarter of SRA.

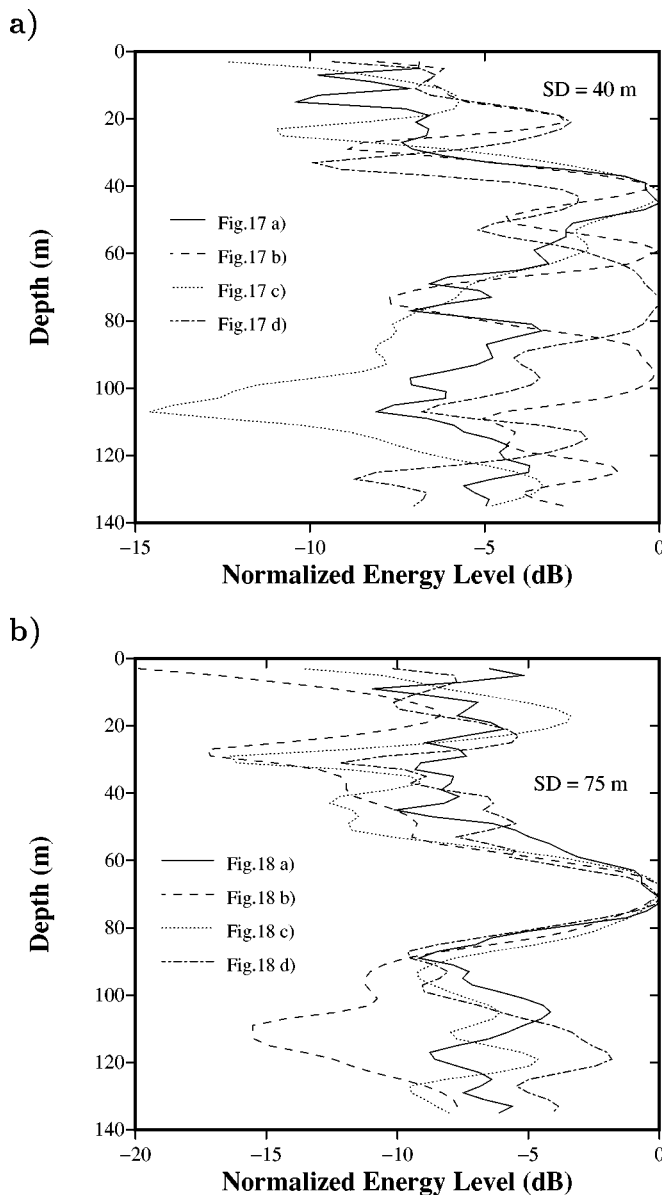


FIG. 19. Energy strength of five-element SRA backpropagation to the VRA. (a) Probe source at 40 m. (b) Probe source at 75 m.

focal distance. Also shown in Fig. 14 is the sound-speed profile taken closest in time to the experimental runs under discussion.

Figure 15 shows backpropagation results initiated from SRA data using (a) the profile obtained from the inversion and (b) the profile taken at the time of the TRM experiment. Clearly, the single experimental profile does not represent a range-independent profile descriptive of the experimental acoustic results, whereas the profile derived from the inversion represents an adequate range-independent approximation to the structure of the water column. These results are also meaningful in the context of mismatch in matched-field processing. The experimental results indicate that a matched field processor using the measured profile would not localize the source.

B. Reduced and sparse aperture TRM

A reduced aperture SRA would enhance the practicality of an ocean TRM. We have already shown through simula-

tion of a harmonic source in Fig. 4(c) that we can expect the phase conjugation process to remain effective as a focusing procedure as aperture is reduced. We should be able to reliably estimate the focal properties of a TRM using data from a subset of source/receiver elements and simulations of the backpropagation using the effective soundspeed profile shown in Fig. 14 found from the inversion. Of course, direct measurement for the sparse arrays would best study this aspect of the TRM, but such data were not taken in this experiment.

Figure 16 shows the results of an adiabatic mode model backpropagation of time-reversed pulse data from every other element of the SRA. We see that for both PS depths the focal region remains prominent for the ten-element SRA. We also present some results for an assortment of five element arrays in Figs. 17 and 18. Figure 19 shows a prediction of the vertical profile of the energy strength of these results which use five element subsets of SRA elements. The results are extended in depth to show the fields near the boundaries. The key thing to notice is that there are some very small arrays which still produce significant concentration of sound in the desired focal region. This probe source depth-dependent result has practical ramifications for active sonar system concepts in which one desires to minimize boundary reverberation at the range of the target. These results are not conclusive for the 40-m probe source depth because that was the depth of more or less maximum variation of the sound-speed profile. Hence, the sound-speed inversion result used in the backpropagation calculation might be the cause of the poorer focusing of the shallow source.

IV. CONCLUSIONS

We have constructed a time-reversal mirror (TRM) in the ocean and hence demonstrated that phase conjugation (PC) is realizable in the ocean using a source–receive array and rather simple signal processing. The waveguide nature of the ocean enhances the focusing properties over a free-space environment because the boundaries in effect enlarge the TRM aperture through its images. The degree of focusing is in excellent agreement with theory. Furthermore, an effective TRM need not be a full water column array. We also have investigated the stability of the PC process *vis a vis* ocean fluctuations and measurements suggest a relatively long stability of the PC process. Future studies will be aimed at the detailed relationship between ocean variability and the PC process and an investigation into the possibility of using PC for inverting for the ocean environment. In addition, it should be straightforward to experimentally confirm predictions of the focal size versus SRA aperture.

ACKNOWLEDGMENT

This research was supported by the Office of Naval Research Code 321US, Contract No. N00014-96-D-0065.

APPENDIX A: FACTORS AFFECTING THE FOCUS

In interpreting the results of the 1996 phase conjugation experiment, a primary issue is degradation of phase-conjugate focusing. Such degrading influences can be di-

vided into static and dynamic categories, the former including propagation and array structure effects and the latter including effects due to the time-varying ocean surface and volume. The object of study is the field produced by a phase conjugate source–receiver array (SRA), which can be written in the general form

$$P_{pc}(r, z; \omega) = \sum_{j=1}^J G_2(\mathbf{r}, \mathbf{r}_j) G_1^*(\mathbf{r}_j, \mathbf{r}_s). \quad (\text{A1})$$

In Eq. (A1), $P_{pc}(r, z; \omega)$ is the field produced at the field point, $\mathbf{r}=(r, z)$, by the phase-conjugate array with probe source placed at $\mathbf{r}_{ps}=(R, z_{ps})$. The sum is over the J elements of the SRA whose position vectors are denoted $\mathbf{r}_j=(0, z_j)$. Following the convention used in the main text, horizontal ranges are measured from the SRA. Propagation from the probe source to the array is described by the Green's function $G_1(\mathbf{r}_n, \mathbf{r}_{ps})$, while propagation from the array to the field point is described by $G_2(\mathbf{r}, \mathbf{r}_n)$. The subscripts 1 and 2 allow for the possibility that time variation of the ocean might cause changes in the Green's function between the probe and phase-conjugate transmission cycles. During either propagation cycle, the ocean is assumed to be “frozen” in the sense that it behaves as a time-invariant linear system. In this view, the Green's function is the frequency-dependent system transfer function for acoustic propagation between any two points in the ocean. The frequency argument of the Green's function used in the main text is suppressed here for convenience, but it becomes important in treating pulsed transmissions.

1. Phase conjugation in static environments

The factors that control phase-conjugate focusing in static environments will be examined by considering a general nonuniform, nonadiabatic waveguide. The conditions for “ideal” phase-conjugate focusing in such a waveguide will be derived and this will implicitly identify the factors that degrade focusing. To simplify the discussion, only vertical phase-conjugate arrays will be considered. The main objective is to generalize Eq. (9) of the main text to the range-dependent case, using the approach given by Siderius *et al.*²² in connection with the “guide source” concept. In this approach, small regions near the probe source and SRA are assumed to be range independent, but the larger region between is allowed to have arbitrary range dependence in bathymetry and sound speed. Losses are neglected and will be discussed later in qualitative terms.

The Green's function for the probe field near the probe source is approximated using range-independent normal modes.

$$G_\omega(r, z; R, z_{ps}) = \sum_n \frac{a_n(z_{ps}) u_n(R, z)}{\sqrt{k_n(R)} |r - R|} e^{ik_n(R)|r - R|}. \quad (\text{A2})$$

Similarly, the Green's function for the probe field at the SRA is written in the form

$$G_\omega(0, z_j; R, z_{ps}) = \sum_n \frac{b_n(z_{ps}) u_n(0, z_j)}{\sqrt{k_n(0)} R} e^{ik_n(0)R}. \quad (\text{A3})$$

The modal eigenfunctions in the vicinity of the probe source and SRA are denoted $u_n(R, z)$ and $u_n(0, z)$, respectively. The corresponding eigenvalues are $k_n(R)$ and $k_n(0)$. These Green's functions do not bear the subscripts 1 and 2 introduced earlier because a time-invariant environment is under consideration. The subscript ω is used here in the same sense as in the main text. The mode amplitudes for the near-source Green's function are

$$a_n(z_{ps}) = \frac{ie^{-i\pi/4}}{\sqrt{8\pi\rho(z_{ps})}} u_n(R, z_{ps}), \quad (\text{A4})$$

and the mode amplitudes for the Green's function near the SRA are given by the linear transformation

$$b_m(z) = \sum_n U_{mn} a_n(z). \quad (\text{A5})$$

For convenience, it is assumed that there are the same number of modes near the source and near the array, so that U_{mn} is a square matrix. Cases for which these numbers are similar but not equal can be treated by discarding high-order modes. The matrix U_{mn} includes any mode coupling that is due to the range dependence of the ocean and is defined in such a way as to be independent of source depth. Furthermore, to the extent that absorption loss in the water column and sea-floor can be neglected, U_{mn} is unitary.

The field produced by the SRA is

$$P_{pc}(r, z; \omega) = \sum_{j=1}^J G_\omega(r, z; 0, z_j) G_\omega^*(0, z_j; R, z_{ps}). \quad (\text{A6})$$

The Green's function for propagation from the j th array element to the field point (r, z) can be expressed in terms of the Green's function for propagation in the opposite direction by using reciprocity:

$$G_\omega(r, z; 0, z_j) = \frac{\rho(z)}{\rho(z_j)} G_\omega(0, z_j; r, z). \quad (\text{A7})$$

In terms of mode amplitudes,

$$G_\omega(r, z; 0, z_j) = \frac{\rho(z)}{\rho(z_j)} \sum_n \frac{c_n(z) u_n(0, z_j)}{\sqrt{k_n(0)} r} e^{ik_n(0)R}, \quad (\text{A8})$$

where the mode amplitudes, $c_n(z)$, are

$$c_m(z) = \sum_n U_{mn} a_n(z) e^{ik_n(R)(r-R)}. \quad (\text{A9})$$

Note that the mode amplitudes, $c_n(z)$, are essentially the same as the $b_n(z)$, but with the source range coordinate shifted by $r - R$.

Equations (A3) and (A8) can be inserted in Eq. (A6) to obtain an expression for the phase-conjugate field in a range-dependent waveguide:

$$P_{pc}(r, z; \omega) = \frac{\rho(z)}{\sqrt{Rr}} \sum_{m,n} \frac{c_m(z) \Delta_{mn} b_n^*(z_{ps})}{\sqrt{k_m(0)} k_n^*(0)} e^{i[k_m(0) - k_n^*(0)]R}, \quad (\text{A10})$$

where

$$\Delta_{mn} = \sum_{j=1}^J \frac{u_m(0, z_j) u_n(0, z_j)}{\rho(z_j)}. \quad (\text{A11})$$

In the ideal case, the array spans the entire water column with elements having uniform spacing, d_a , and the modal eigenfunctions have negligible amplitude in the bottom. In this case, the sum over array elements in Eq. (A11) approximates the orthogonality integral for modal eigenfunctions [Eq. (5)], and $\Delta_{mn} d_a$ can be taken equal to δ_{mn} . This ideal can be approached quite closely in the environment of the 1996 experiment. Using the environmental parameters defined in Fig. 4(a), and considering only the first 12 modes, an array with 36 elements with spacing $d_a = 3.33$ m and with the shallowest element 4.44 m below the surface gives diagonal elements in $\Delta_{mn} d_a$ that are within 3% of unity and off-diagonal elements that are of order 0.03 or less. The first mode is an exception; it has a small diagonal element as it is trapped in the first sediment layer and not adequately sampled by the array. This is of no consequence, as this mode is very lossy and does not contribute to propagation. The element placement of the actual array gives smallest diagonal elements of about 0.5 with a few off-diagonal elements as large as 0.3.

Returning to the derivation of the conditions for ideal phase-conjugate focusing, take $\Delta_{mn} = \delta_{mn}/d_a$ in Eq. (A10) to obtain

$$P_{pc}(r, z; \omega) = \frac{\rho(z)}{d_a \sqrt{Rr}} \sum_{m,n} Q_{mn} a_m(z) a_n^*(z_{ps}) e^{ik_m(R)(r-R)}, \quad (\text{A12})$$

where

$$Q_{mn} = \sum_l \frac{U_{lm} U_{ln}^*}{k_l(0)} e^{-2\Im[k_m(0)]R}. \quad (\text{A13})$$

Losses due to absorption and scattering are detrimental to phase-conjugate focusing, as they cause attenuation of higher-order modes, yielding a blurrier focus than would be possible with lower loss. Furthermore, this blurring will increase as the range between the source and the array increases owing to the strong range and mode number dependence of attenuation. Thus in defining the ideal case, losses are set to zero and the mode coupling matrix, U_{mn} , is taken to be unitary. If the mode dependence of $k_l(0)$ in Eq. (A13) is neglected,

$$Q_{mn} = \frac{\delta_{mn}}{k_m(0)}, \quad (\text{A14})$$

and the phase-conjugate field for an ideal array in a lossless environment can be approximated as

$$P_{pc}(r, z; \omega) = \sum_n \frac{u_n(R, z) u_n(R, z_{ps}) e^{ik_n(R)(r-R)}}{8\pi\rho(z_{ps})k_n(0)d_a\sqrt{Rr}}. \quad (\text{A15})$$

Apart from inessential factors, this expression is the same as Eq. (9) of the main text which was derived for the range-independent case. Even though Eq. (A15) represents the ideal case, it illustrates properties that actual phase-conjugate arrays may possess, provided they are not too far from ideal.

One such property is independence of the focus pattern on the distance between the probe source and the array (when absorption can be neglected and apart from the cylindrical spreading factor $1/\sqrt{Rr}$). Even more strikingly, the focus field is independent of the (possibly range-dependent) environment between the focus and the array (see examples presented by Siderius *et al.*²²). That is, the focus depends only on the local properties of the water column and sea floor and is not affected by bathymetry or range-dependent water column properties in the region between the array and the focus, provided the latter do not change appreciably during the two propagation cycles. This means that, in the ideal case, phase conjugation is not affected by time-invariant forward scattering due to bathymetry, fronts, etc. It also implies that, in simulations of phase-conjugate focusing, it is important to accurately model the ocean in the vicinity of the focus, but less accuracy is required for the more distant parts of the propagation path. One important reservation must be added at this point. The derivation above is essentially two dimensional in that cross-range spatial variation of the ocean is neglected. Static out-of-plane scattering will degrade phase-conjugate focusing if one-dimensional vertical arrays are used. Planar or volumetric arrays of sufficient aperture, on the other hand, will not suffer due to static out-of-plane scattering.

The invariance seen in the ideal case is similar to that predicted for an ideal, closed phase-conjugate surface array⁴ which produces a strictly invariant focal field that resembles the original field of the probe source, except that the phase-conjugate field is a standing wave. In the present case, the probe source field (including only propagating modes) is given by Eq. (A2) which can be put in the form

$$G(r, z; R, z_{ps}) = \frac{ie^{-i\pi/4}}{\rho(z_{ps})\sqrt{8\pi|r-R|}} \times \sum_n \frac{u_n(R, z) u_n(R, z_{ps}) e^{ik_n(R)|r-R|}}{\sqrt{k_n(R)}}. \quad (\text{A16})$$

Apart from a difference in spreading loss and an overall phase difference, Eqs. (A15) and (A16) are quite similar. There is a slight term-by-term difference owing to differing factors involving modal eigenvalues, but the primary difference is in the propagation phase factor. The source field propagates *away* from the source location while the phase-conjugate field propagates *past* the source location in the direction away from the array.

2. Phase conjugation in time varying environments

Time-dependent forward scattering due to surface and internal waves causes change in the propagation characteristics of the medium in the time interval between the probe and phase-conjugate transmission cycles with attendant degradation of phase-conjugate focusing.⁵ In discussing scattering from a general point of view, it is convenient to decompose the Green's function into coherent and incoherent parts:

$$G_\alpha(\mathbf{r}, \mathbf{r}') = \bar{G}(\mathbf{r}, \mathbf{r}') + \delta G_\alpha(\mathbf{r}, \mathbf{r}'). \quad (\text{A17})$$

The subscript α takes on the values 1 and 2 for the probe and conjugate transmission cycles, respectively. The coherent, or mean, Green's function, $\bar{G}(\mathbf{r}, \mathbf{r}')$ is not assigned a subscript because the random time variations are assumed to be stationary in the statistical sense. It will be assumed that sufficient time has elapsed between the probe and conjugate transmission cycles that variations in the two Green's functions are uncorrelated.

$$\langle \delta G_2(\mathbf{r}_d, \mathbf{r}_c) \delta G_1^*(\mathbf{r}_b, \mathbf{r}_a) \rangle = \langle \delta G_2(\mathbf{r}_d, \mathbf{r}_c) \delta G_1(\mathbf{r}_b, \mathbf{r}_a) \rangle = 0. \quad (\text{A18})$$

This condition was very likely satisfied in the 1996 experiment with respect to scattering by surface waves, which have correlation timescales on the order of seconds, while the time between transmission cycles was measured in minutes and hours. Internal waves have relatively long correlation time scales, but the longer transmission intervals (several minutes to a few hours) of the experiment were most likely sufficient to produce decorrelation of fluctuations in volume scattering.

Combining Eqs. (A1), (A17) and (A18), the mean phase-conjugate field is

$$\bar{P}_{pc}(r, z; \omega) = \sum_{j=1}^J \bar{G}(\mathbf{r}, \mathbf{r}_j) \bar{G}^*(\mathbf{r}_j, \mathbf{r}_{ps}), \quad (\text{A19})$$

and the variance of the field is

$$\begin{aligned} & |\overline{P_{pc}(r, z; \omega)}|^2 - |\bar{P}_{pc}(r, z; \omega)|^2 \\ &= \sum_{j=1}^J \sum_{j'=1}^J [\bar{G}(\mathbf{r}, \mathbf{r}_j) \bar{G}^*(\mathbf{r}, \mathbf{r}_{j'}) K_{jj'}(\mathbf{r}_{ps}) \\ &+ \bar{G}(\mathbf{r}_{ps}, \mathbf{r}_j) \bar{G}^*(\mathbf{r}_{ps}, \mathbf{r}_{j'}) K_{jj'}(\mathbf{r}) + K_{jj'}(\mathbf{r}) K_{jj'}(\mathbf{r}_{ps})], \end{aligned} \quad (\text{A20})$$

where

$$K_{jj'}(\mathbf{r}) = \langle \delta G_\alpha(\mathbf{r}_j, \mathbf{r}) \delta G_\alpha^*(\mathbf{r}_{j'}, \mathbf{r}) \rangle. \quad (\text{A21})$$

The covariance, $K_{jj'}(\mathbf{r})$, is proportional to the correlation between the incoherent field at elements j and j' of the array with a unit point source situated at \mathbf{r} . In deriving Eq. (A20), free use was made of reciprocity (which allows interchange of the two arguments of the Green's function) and stationarity (which means that δG_1 and δG_2 have identical statistics).

Equations (A19) and (A20) are general and include three-dimensional scattering (i.e., in-plane and out-of-plane scattering). They lead to two general conclusions regarding focusing in the 1996 experiment for those cases in which sufficient time elapsed between the two transmission cycles. First, the mean focus field, that is, the focus field averaged over many independent probe-conjugate-transmission cycles, is obtained by using the coherent Green's function in place of the actual (random) Green's function. Second, and most important, the field near the focus does not fluctuate appreciably, that is, it is well approximated by the mean focus field. This conclusion is supported by careful inspection of Eq. (A20), which shows that the variance of the phase-conjugate field is not localized near the focus, but is spread diffusely in range and depth. Thus near the focus, the mean

field dominates, unless scattering is strong enough to diminish the mean Green's function to such a degree that focusing is essentially destroyed.

To see that the field variance is unfocused, it is necessary to discuss each term in Eq. (A20). The first term can be viewed as being proportional to the intensity of a phase reversed retransmission of the incoherent field produced by scattering of the probe transmission. This retransmission will be directed back toward the scatterers responsible for the incoherent component of the probe field, and these are spread over the entire volume and surface of the ocean. Similarly, the second term is proportional to the intensity produced at the source location by a coherent retransmission of the phase-reversed incoherent field produced from a fictitious source placed at the field point (reciprocity is being used in this interpretation). Again, this retransmission will be diffuse and will not peak as the field point approaches the source location. The last term in Eq. (A20) is more difficult to assess. It is a double sum over all array elements of the product of covariances due to sources placed at both the field point and probe source location. If scattering and propagation are very complicated in a spatial sense, these covariances will not be strongly dependent upon the source locations. That is, the incoherent field produced by these sources does not contain information on the source location. If this is the case, the covariances will be largely independent of \mathbf{r} and \mathbf{r}_{ps} , and the last term of Eq. (A20) will not peak as \mathbf{r} approaches \mathbf{r}_{ps} .

APPENDIX B: HARDWARE DESCRIPTION

The phase conjugation (time reversal mirror) experiment was carried out in April 1996 off the northwest coast of Italy. As shown in Fig. 2, a source-receiver array (SRA) was deployed in 125-m-deep water and cabled approximately 1 km back to a small island, Formica di Grosseto (42° 34.6' N, 10° 52.9' E). A rf telemetered vertical receive array (VRA) was deployed in 145-m-deep water approximately 6.3 km west of Formica and used to measure the structure of the acoustic field across the water column. The R/V ALLIANCE received this rf telemetered data stream and also deployed a source-receive transponder (SRT) (echo repeater) which also was used as a probe source (PS).

The vertical source array portion of the SRA consisted of 24 slotted cylinder sources spaced 3.33 m apart (total aperture 76.6 m). The sources have a resonance at approximately 445 Hz and a 3 dB bandwidth of approximately 35 Hz as shown in Fig. B1. Thus the SRA sources were separated by approximately one wavelength at their center frequency. Each source was hardwired individually back to the transmit control system on Formiche di Grosseto via a multiple twisted pair umbilical cable. The transmit control system synthesized the low-level analog signals for each source and these then were amplified prior to coupling onto the umbilical cable. Based on a nominal driving level of 100 VRMS, the nominal source level of the transducers was 165 dB *re: μPa*.

In addition to the vertical source array, the SRA included a colocated (i.e., physically strapped together) vertical receive array consisting of 48 hydrophones spaced half the separation of the source array transducers. The time se-

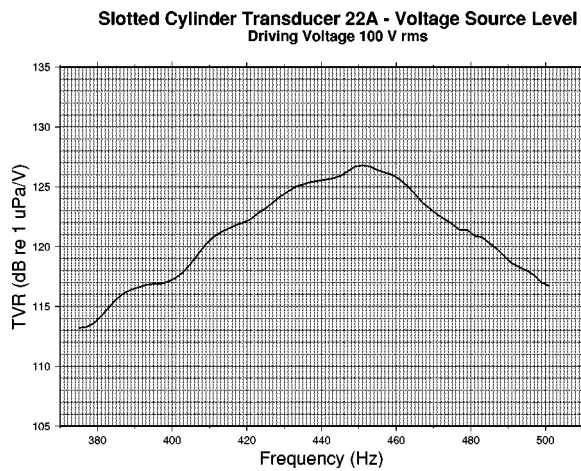


FIG. B1. Transmitting voltage response (TVR) versus frequency for one of the slotted cylinder source array transducers.

ries from each array element was sampled at $f_s = 1.5$ kHz using 24 bit A/D converters, multiplexed onto a single digital data stream, and cabled back to Formiche di Grosseto via a separate coaxial umbilical cable.²³ The shore-based digital data acquisition system archived the data stream and enabled capturing short segments of the array time series (from the 24 hydrophones colocated with the source array transducers) for time reversal and retransmission by the transmit control system. Due to high-level contaminants observed in four of the time series, these channels were set to zero during the retransmission process.

The rf telemetered vertical receive array (VRA) consisted of 64 hydrophones in a nested configuration over a 90-m aperture.²⁴ A 46 element subset of these hydrophones with 2-m spacing was used to generate the results discussed in the main text. The time series from each array element was sampled at $f_s = 1.2$ kHz, multiplexed onto a single digital data stream, and sent via rf telemetry to the R/V ALLIANCE for both quick-look analysis and archival purposes.

Last, the source–receive transponder (SRT) (echo repeater) and probe source (PS) consisted of a slotted cylinder transducer identical to those used in the source array, and it was operated at the same nominal source level of 165 dB re: 1 μ Pa. When used as an echo repeater, the SRT included a separate receiving hydrophone to sample the acoustic field at the depth of the source. In this case, a short segment of the received time series containing a SRA transmission was captured, amplified, and retransmitted (without time reversal). When used simply as a source, the SRT transmitted a 50-ms, 445-Hz pulse which probed the multipath structure of the channel. In this case, the SRA received the temporally and spatially spread transmission, time reversed and amplified the 24 time series, and retransmitted them from the source

array transducers. By allowing the R/V ALLIANCE to tow the PS slowly through the range between the SRA and VRA, the focal region of the phase conjugation process could be studied and these results are discussed in the main text.

- ¹B. Y. Zel'dovich, N. F. Pilipetsky, and V. V. Shkunov, *Principles of Phase Conjugation* (Springer-Verlag, Berlin, 1985).
- ²M. Fink, C. Prada, F. Wu, and D. Cassereau, "Self-focusing with time reversal mirror in inhomogeneous media," *Proc. IEEE Ultrason. Symp.* 1989 Montreal **2**, 681–686 (1989).
- ³M. Fink, "Time Reversal Mirrors," in *Acoustical Imaging*, Vol. 21, edited by J. P. Jones (Plenum, New York, 1995), pp. 1–15.
- ⁴D. R. Jackson and D. R. Dowling, "Phase conjugation in underwater acoustics," *J. Acoust. Soc. Am.* **89**, 171–181 (1991).
- ⁵D. R. Jackson and D. R. Dowling, "Narrow-band performance of phase-conjugate arrays in dynamic random media," *J. Acoust. Soc. Am.* **91**, 3257–3277 (1992).
- ⁶D. R. Dowling, "Phase-conjugate array focusing in a moving medium," *J. Acoust. Soc. Am.* **94**, 1716–1718 (1993).
- ⁷D. R. Dowling, "Acoustic pulse compression using passive phase-conjugate processing," *J. Acoust. Soc. Am.* **95**, 1450–1458 (1994).
- ⁸A. Parvulescu and C. S. Clay, "Reproducibility of signal transmissions in the ocean," *Radio Electron Eng.* **29**, 223–228 (1965).
- ⁹A. Parvulescu, "Matched-signal ("Mess") processing by the ocean," *J. Acoust. Soc. Am.* **98**, 943–960 (1995).
- ¹⁰A. B. Baggeroer, W. A. Kuperman, and P. N. Mikhalevsky, "An overview of matched field methods in ocean acoustics," *IEEE J. Ocean Eng.* **18**, 401–424 (1993).
- ¹¹F. B. Jensen, "Sound propagation in shallow water: A detailed description of the acoustic field close to the surface and bottom," *J. Acoust. Soc. Am.* **70**, 1397–1406 (1981).
- ¹²F. B. Jensen, W. A. Kuperman, M. B. Porter, and H. Schmidt, *Computational Ocean Acoustics* (American Institute of Physics, New York, 1994).
- ¹³M. B. Porter, "The KRAKEN normal mode program," *SACLANTCEN Memorandum, SM-245*, La Spezia, Italy (1991).
- ¹⁴R. K. Brienzo and W. S. Hodgkiss, "Broadband matched-field processing," *J. Acoust. Soc. Am.* **94**, 2821–2831 (1993).
- ¹⁵W. A. Kuperman and F. Ingenito, "Attenuation of the coherent component of sound propagating in shallow water with rough boundaries," *J. Acoust. Soc. Am.* **61**, 1178–1187 (1977).
- ¹⁶C. Prada, F. Wu, and M. Fink, "The iterative time reversal mirror: A solution to self-focusing in the pulse echo mode," *J. Acoust. Soc. Am.* **90**, 1119–1129 (1991).
- ¹⁷C. Prada, J. L. Thomas, and M. Fink, "The iterative time reversal process: Analysis of the convergence," *J. Acoust. Soc. Am.* **97**, 62–71 (1995).
- ¹⁸C. Prada, S. Manneville, D. Spoliansky, and M. Fink, "Decomposition of the time reversal operator: Detection and selective focusing on two scatterers," *J. Acoust. Soc. Am.* **99**, 2067–2076 (1996).
- ¹⁹A. Tolstoy, "Linearization of the matched field processing approach to acoustic tomography," *J. Acoust. Soc. Am.* **91**, 781–787 (1992).
- ²⁰M. D. Collins and W. A. Kuperman, "Focalization: Environmental focusing and source localization," *J. Acoust. Soc. Am.* **90**, 1410–1422 (1991).
- ²¹A. Tolstoy, *Matched Field Processing for Underwater Acoustics* (World Scientific, Singapore, 1993).
- ²²M. Siderius, D. R. Jackson, D. Rouseff, and R. P. Porter, "Multipath compensation in range dependent shallow water environments using a virtual receiver," *J. Acoust. Soc. Am.* (submitted).
- ²³W. S. Hodgkiss, J. C. Nickles, G. L. Edmonds, R. A. Harriss, and G. L. D'Spain, "A large dynamic range vertical array of acoustic sensors," in *Full Field Inversion Methods in Ocean and Seismic Acoustics*, edited by O. Diachok, A. Caiti, P. Gerstoft, and H. Schmidt (Kluwer Academic, Dordrecht, The Netherlands, 1995), pp. 205–210.
- ²⁴L. Troiano, P. Guerrini, and A. Barbagelata, "SACLANTCEN towed and vertical array system characteristics" (1995).